Journal of Applied Engineering Mathematics

Volume 11, December 2024

Parameter Optimization for Valid Assumption of Infinite Length in Molten Salt Measurement System

Spencer Larson, Jacob Numbers

Mechanical Engineering Department
Brigham Young University
Provo, Utah 84602
lspenc17@byu.edu, jacobcn2@student.byu.edu

Abstract

A modified transient hot-wire ”needle probe” device is a proposed method for measuring the thermal conductivity of reactor-grade nuclear salts. The assumption of 1-dimensional heat transfer in the analytical model used to solve for λ and other sample properties is evaluated, using FlexPDE to evaluate the heat diffusion equation for a thermal quadrupoles model. Analysis shows that the current length-to-diameter ratio in the testing region justifies an infinite cylinder approximation. For FLiNaK, water, and argon, the proportion of heat flux emitted in the axial direction is shown to be negligible during typical testing time frames. Due to sensitivity to power input, further development is recommended. Argon gas does not show significantly more radial to axial heat losses compared to FLiNaK or water. As free convection may play a larger role heat transfer for argon gas than for liquids, addition analysis is recommended.

Nomenclature

COMSOL - Multi-physics finite-element simulation software. FlexPDE - Finite element model builder and solver. FLiNaK - A blend of lithium-fluoride, sodium-fluoride, and potassium-fluoride proposed for use in next-generation molten salt nuclear reactors. MSTDB - Molten Salt Thermal Properties Database

Introduction

Molten salts have seen increased attention for use in applications ranging from large-scale thermal storage and heat transfer to waste processing [17, 6, 16]. Renewed interest in molten salts has grown particularly relating to their use in next-generation nuclear power plants. The operable temperature range of molten salts as a heat transfer fluid in nuclear reactors would enable significant advantages in safety [12] and efficiency [2]. Stringent regulation requires comprehensive predictive modeling of the molten salt reactors, which is currently inhibited by the lack of thermophysical property data.

Of the thermophysical properties of molten salts included in the Molten Salt Thermal Properties Database (MSTDB) [15], thermal conductivity has the highest property uncertainty and is the least measured. It has also been shown to be one of the most critical parameters for accurate reactor modeling in terms of safety and performance [13]. The challenges of handling molten salts—including a high oxidation potential and electrical conductivity—make thermal conductivity measurements especially challenging. Many procedures have been devised to measure

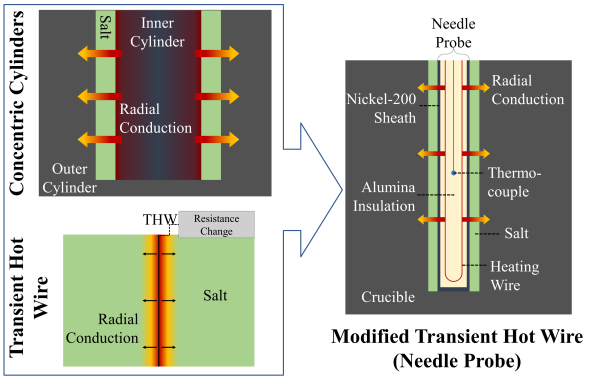

Figure 1: Modified transient hot-wire "needle probe" device

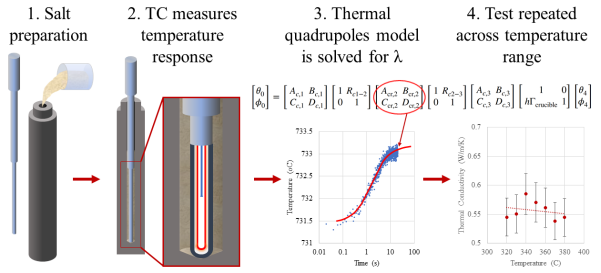

Figure 2: Measurement process of molten salt thermal conductivity using needle probe.

molten salt thermal conductivity [7], though no standardized method exists.

A modified combination of the transient hot-wire and concentric cylinders method was developed by Merritt et. al [10]. Termed the "needle probe", the device avoids electrical interference by electrically insulating a thermocouple and heating wire within AlO_2 ceramic, which is sheathed in nickel to form a long needle-like probe. The probe is situated concentrically within a crucible, creating a thin annulus of the sample to be measured (see Figure 1). The narrow gap (< 0.7mm) controls the onset of free convection which has been shown to be effectively eliminated at narrow gap sizes [3]. The crucible and probe are placed within a furnace under an argon atmosphere, and brought to steady state temperature above the melting point. A voltage is applied to the internal heating wire of the probe to generate Joule heating as the internal thermocouple measures the transient temperature response with time. The experimental data is then fitted to a thermal quadrupoles analytical model [8] of the probe-crucible setup, where the properties of the salt are then solved for via an inverse Laplace transform numerical MATLAB solver [4, 5]. The testing region of the needle probe (the length of heating wire with the thermocouple at the axial center) is only 10cm in length and <2.5cm in diameter—the small scale of the probe and the transient nature of the test greatly reduces run times, allowing an entire temperature range to be measured in a single day. Depending on the sample's thermal conductivity, the time range needed ranges from 15-45 seconds. The data collection and solution process is summarized in Figure 2.

The thermal quadrupoles technique describes heat conduction according to Fourier's law in terms of Bessel functions with a system of equations describing the temperature and flux at the inner and outer layer of each surface, allowing the model to describe the multilayered cylindrical probe setup [8, 10]. The analytical model also takes into account the radiative heat transfer between the surface of the probe and the crucible, with reasonable assumptions regarding the optic properties of the molten salts. The model assumptions define the heat generation of the inmost cylinder (lumped heating wire) as a constant heat source, with a heat flux of 0 at the external boundary. The probe is also considered to be an infinitely long rod, assuming heat generation is uniform at the thermocouple axial height. In supplying the model parameters, the value of the heat source is taken to be the heating power of the wire, i.e. voltage multiplied by the current $VI = Q$, which are collected from sensors at the probe.

Despite successful measurements of fluoride, chloride, and nitrate salts[9, 11], several challenges interfere with extensive implementation of the device. The thermal quadrupoles model relies on the assumption of 1-dimensional radial heat diffusion, and does not account for axial heat losses in the case of a low-thermal conductivity samples. The assumption of infinite length has also not been justified in terms of the ideal length-diameter ratio of the probe, which has been suggested should exceed 50 [1]—far greater than the ratio of 4 that exists for the needle probe. Additionally, changes to the physical device resultant of thermal cycling and regular wear and tear have led

to deviations from the analytical model, which are difficult to diagnose due to the complex heat transfer dynamics of the probe's internal layers. In the absence of a calibration fluid that spans the operating temperature range, other thermal conductivity measurement methods have used inert gases (whose conductivity is well established in literature) [15]. This poses challenges to the 1-dimensional model of the needle probe, in which the relatively lower thermal conductivity of argon (used in the glovebox for needle probe measurements) may drive a larger axial to radial heat flux ratio. Merritt et. al. proposed via COMSOL model simulations of an identical probe that, in the case of toluene ($k = 0.13 W m^{-1} K^{-1}$), the radial to axial heat flux ratio approached 5 after 40 seconds of heating [10]. However, the cited source does not indicate which points were used in the calculation of axial and radial heat fluxes. Determining whether or not this invalidates the assumption of uniform heating for an argon sample is required to justify an argon calibration approach. To reliably model the physical system, the heat output crossing the boundary layer of the heating wires must match the input power supplied to the model.

The present study will report on findings regarding the validity of model assumptions and the justifiability of using an argon calibration approach. Finite element analysis, informed by analytical interpretations, will be used to model the needle probe in 2 dimensions. Conclusions from this report will provide the necessary evidence to implement further use of the needle probe method and offer insights for future design iterations.

Methods

The objectives of this study include the following:

1. Calculate the ratio of radial to axial heat fluxes of the needle probe testing apparatus under various temperatures and materials.
2. Determine if the current length-to-diameter ratio of the testing region of the probe justifies an infinite cylinder approximation.
3. Validate the use of argon as a calibration material.

To accomplish these aims, the heat diffusion equation that describes the dynamics of the experiment was developed to allow solution of the relevant heat fluxes and power output. Under the assumption of angular symmetry and the presence of heat generation, the heat diffusion equation reduces to:

$$\frac{1}{r} * \frac{\partial}{\partial r}(r * \frac{\partial T}{\partial r}) + \frac{\partial}{\partial z}(\frac{\partial T}{\partial z}) + \dot{q}(z) = \frac{1}{\alpha}\frac{\partial T}{\partial t} \qquad (1)$$

where temperature T is a function of radius r, axial height z, and time t. In other words, $T(r, z, t)$, where $r_1 \leq r \leq r_2$, $0 \leq z \leq L$, and $0 < t < 100$. Assuming uniform heat distribution along the heating region, the heat flux may be treated as the forcing function in the system, represented by $\dot{q} = q_o * (H(z - z_1) - H(z - z_2)$, where q_o is the power input to the probe's heating wire.

The boundary and initial value conditions are defined by the nature of the transient measurement method. At $t_o = 0$, a voltage is applied to the heating wire of the probe, causing a constant heat flux to radiate outward through the molten salt layer. The initial condition for the system may then be stated as $T(r, z, 0) = T_o$. Per convention of the thermal quadrupoles method, the external heat flux is $\frac{\partial T}{\partial r} = 0$. Sensitivity analyses in COMSOL also verify that at time scales less than 100 s, the convection coefficient at the external boundaries of the control volume of the crucible has a negligible effect on the temperature distribution for all the samples considered (water, toluene, galinstan, $NaNO_3$), allowing for a constant temperature condition $T = T_0$ at the boundaries.

To solve the heat diffusion equation for a cross-sectional area of the system normal to the probe radius, a finite element analysis model was created using the partial differential equation solver FlexPDE v.7 [14]. The FlexPDE solver enables the rapid solution and iteration of the analytical heat diffusion equation over the various boundaries and regions of the system in both axial and radial 2-dimensional domains. Because the axial model assumes uniform heat generation in the lumped cylindrical volume swept by the heating wires around the axis, the radial model was needed to verify that heat generation was uniform at the outer surface of the probe. Even neglecting a probable thermal contact resistance between the nickel sheath and the alumina insulation, heat generation rapidly approaches uniformity at the probe surface in the axial model, validating the assumption of azimuthally uniform heat generation in the radial model (see Figure 3). The radial view of the FlexPDE model was used, from which

solutions were generated for the point heat fluxes, power outputs, and flux profiles at the relevant boundaries. Free convection between the probe and crucible is ignored due to conclusions stated previously. To determine whether argon performed similarly to typical test liquids, calculations were made for water, argon, and molten salt FLiNaK (eutectic LiF-NaF-KF, considered for nuclear molten salt reactor applications) at 20°C (for water and argon) and 600°C (argon and FLiNaK).

Boundary conditions of the individual regions of the system are detailed in the FlexPDE model to which the heat diffusion equation was applied (see code in Appendix C). These include constant volumetric heat generation in the bottom 10cm portion of the heating wire (with a ramped-down condition to avoid discontinuities) and 0 heat flux at the axial position. Only half of the radial view was modeled, and so solutions for the output power output and heat flux are multiplied by a factor of 2 when appropriate.

The transient temperature response was captured for the first 100 s from the start of heat generation. To accurately account for the total radial heat flux, a surface integral was taken at the outer boundary of the heat-generating wire over the entire Z-dimensional, and then divided by the area of the cylinder. The total axial heat flux was similarly calculating by dividing the sum of the top and bottom heat flux surface integrals (placed axially at the top and bottom limits of the heat generation region) by the area of the circular cross-section. These yielded the averaged axial and radial heat fluxes in $Wm^{-1}K^{-1}$, which could then be plotted as a ratio of the radial-axial fluxes with time to observe the degradation of the ratio with test time. These curves also provide a quantitative measurement of deviation between argon gas and liquids to verify its applicability as a calibration fluid.

To determine whether the current length-to-diameter ratio of the testing region can approximate infinite-cylinder behavior, the power output at the heating wire was calculated at the outer boundary of the heating wire at the height of the thermocouple, which (if the radial-axial flux is large) should near the value of the power supplied to the wire in the form of Joule heating. Additionally, a symbolic derivation of the radial flux vector as a function of the resultant flux ratio provided an analytical standard to judge the radial-to-axial heat flux ratio. Combining the results from the computational model and the symbolic analysis, conclusions were then made regarding the infinite length assumptions and the validity of argon as a calibration material.

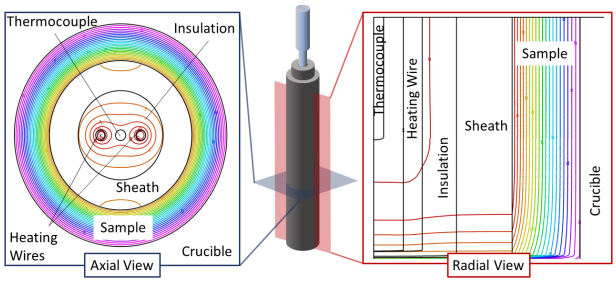

Figure 3: Depiction of 2-dimensional heat transfer modeling via FlexPDE software [14].

Results

A symbolic representation of the axial to radial flux relationship is first developed. Assuming uniform angular heat distribution throughout the molten salt layer, the heat flux at an infinitesimal point on the surface of the heat source can be represented as the vector sum with radial and axial components, as represented by equation (2).

$$\dot{W}_{total} = \sqrt{\dot{W}_{radial}^2 + \dot{W}_{axial}^2} \tag{2}$$

Where $\dot{W}$ is the heat flux in either the axial or radial direction. Rearranging the expression results in Equation (3) (see Appendix A) for the complete derivation) .

$$\dot{W}_{radial} = \dot{W}_{total} * \frac{\dot{W}_{radial}/\dot{W}_{axial}}{\sqrt{\dot{W}_{radial}^2/\dot{W}_{axial}^2 + 1}} \tag{3}$$

Plotting this equation as a function of $\frac{\dot{W}_{radial}}{\dot{W}_{axial}}$—depicted in Figure 4—reveals that once the ratio of radial to axial heat flux exceeds a magnitude of 5, nearly all of the heat flux is emitted in the radial direction. From the previously mentioned sensitivity analysis of the probe performed by Merritt et. al., it was shown that if the radial flux is decreased by ≈-5%, the slope of the temperature profile in the analytical model similarly decreases by ≈-5% [9] along the entire temperature range. A radial-axial

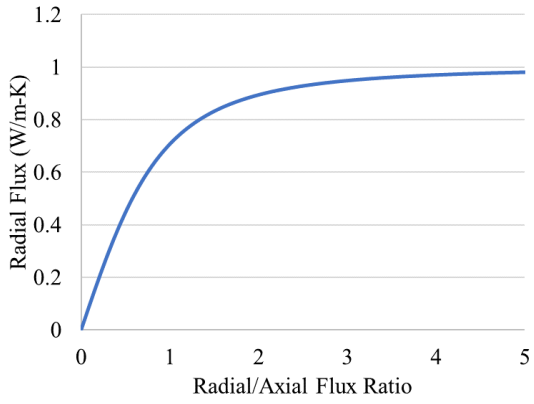

Figure 4: Fraction of the total radial heat flux emitted in the radial direction as a function of the ratio $\frac{\dot{W}_{radial}}{\dot{W}_{axial}}$.

heat flux ratio of 5 yields a radial flux that is 98.06% of the total flux, within the uncertainty limits of the power term. 5 is then considered to be the minimum standard which must be reached by needle probe device.

FlexPDE simulations of water, FLiNaK, and argon are compared to this symbolic derivation. As a qualitative evaluation, it is noted in Figure 5 that the argon solution exhibits a significantly more varied temperature distribution in the sample region compared to the FLiNaK solution, while the FLiNaK solution has a steeper temperature change with axial distance in the region above the heating length. Despite these differences, there appears to be relative uniformity in the temperature profile at the height of the thermocouple (about 0.05m). See Appendix B for a plot of the heat flux distribution.

Figure 6 depicts the FlexPDE calculations of the change in radial to axial heat flux with time for water, FLiNaK, and argon. Despite the variation in thermal conductivities between argon and FLiNaK/water, the ratio of heat flux orientation never dips below the threshold of 5 until 92.5s of heating, and only first for argon at 600 °C; FLiNaK and water never reach below the threshold in the 100s time frame. Despite some variation between the argon and the FLiNaK and water ratios around the 10s mark, the gas is notably similiar to the two liquids, supporting the transferability of argon calibration data as a reference fluid. Given the fact that needle probe tests never require more than 60

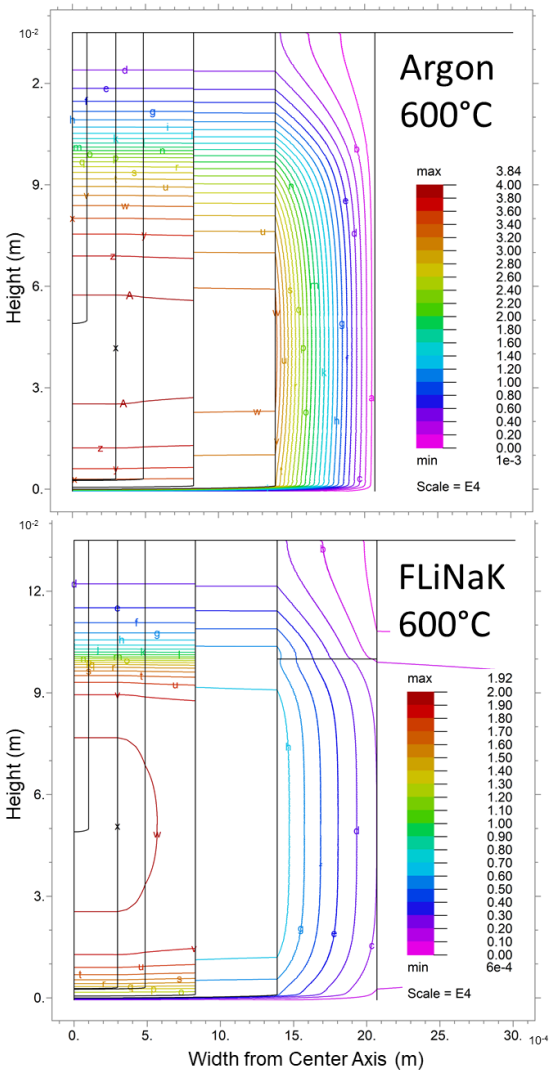

Figure 5: Comparison of FlexPDE temperature distributions for argon and FLiNaK at 600 °C at t=40s.

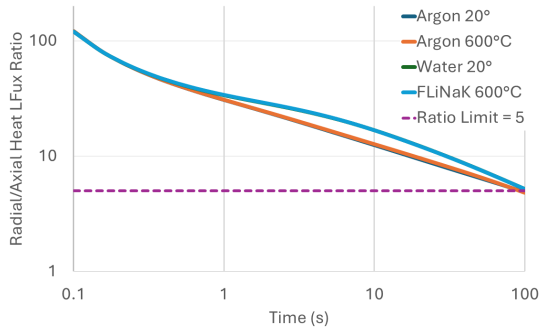

Figure 6: Change in Radial to Axial Heat Flux over time for argon (20°C and 600°C), water (20°C), and FLiNaK (600°C).

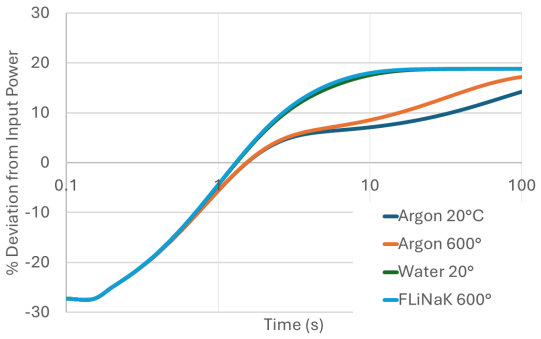

Figure 7: Percent deviation from the input power of the average radial power output calculated from the cylindrical heat generation layer.

seconds of data (at which the point the ratio ranges from 98.66-98.98% among the four materials), falling below a ratio of 5 according to the symbolic derivation of equation (3) is not a risk with the current length-diameter ratio.

To evaluate whether the power output at the heating wire layer surface is equivalent to the supplied power used in the thermal quadrupoles analytical model, the average power output at a 1-dimensional line extending from the heating wire radially was plotted by its percent deviation from the constant value supplied power, as shown in Figure 7. Despite the existence of axial losses, the plot indicates that the average radial power output exceeds the input power; it should be lower if such were the case. It is noted that in calculating the average power output, the surface integral of the heat flux at the outer radius of the heating wire was calculated from the axial z-values that spanned the upper limit where heat generation occurs to the bottom of the curved portion of the heating wire. While this may provide a reasonable accounting of the area over which the heat generating wires will transfer heat radially, it does not capture any portions of the heat flux that may flow radially after first diffusing axially (see again Appendix B). Additionally, the curved portion at the bottom loop of the heating wire is ignored in the averaging calculation due to the nature of the cylindrical surface integral. Precisely because the heat flux along the axis is not uniform (particularly at the extrema of the heating length), back-calculating the 1-dimensional power output over the complex area of the heating wire may introduce losses that result in the apparent deviation ranges from -38% to 18%, where minor miscalculations in the volumetric heating can cause substantial differences. A more robust calculation would be to calculate the heat flux at the surface of the heating wire and then divide it by the area of the finite element parallel to the surface. FlexPDE does not readily provide this, and so the improvement is left as a suggestion for further study.

Conclusions

To increase the reliability and throughput of molten salt thermal conductivity measurements, the modified transient hot-wire ”needle probe” device [10] was evaluating for its assumption of 1-dimensional heat transfer in the analytical model used to solve for λ and other sample properties. The heat diffusion equation was solved for the needle probe system using computational analysis in FlexPDE [14]. A general vector derivation of radial to axial heat fluxes was used to establish a lower limit of the radial to axial heat fluxes of 5. It was shown that for FLiNaK, water, and argon, this threshold was never crossed during typical testing time frames. Evaluations of the actual heat source in comparison to the constant power supplied to the 1-D thermal quadrupoles model of the system was inconclusive due to the inaccuracy of averaging the heat flux over the entire heating region. It is suggested for further development to instead calculate the heat flux and area of

an appropriate finite element, and compare this result with time to the supplied power.

The results of the comparison of the radial to axial heat fluxes for the stated materials indicate that, despite variation in temperature profiles, argon does not exhibit significantly more radial to axial heat losses in comparison to the higher conductivity fluids FLiNaK and water. This suggests that an argon calibration approach is valid. Further studies should examine the relative potential of free convection in argon gas—while this can be reasonably neglected for liquids, it has not been justified for gases. From these studies, it was also observed that the current needle probe's length-to-diameter ratio of 5 provides a sufficient radial-axial heat flux ratio, contrary to some sources that suggest a length-to-diameter ratio of 50 is required at a minimum [1]. Further investigation should consider an optimization of the minimum ratio, which would inform future needle probe iterations and other similar devices.

Acknowledgements

We would like to acknowledge the efforts of Troy Munro, Brian Merritt, and Ryan Ruth, who have all contributed to the development of this project.

References

[1] G. Bovesecchi, P. Coppa, and S. Pistacchio. "A new thermal conductivity probe for high temperature tests for the characterization of molten salts". In: *Review of Scientific Instruments* 89.5 (May 2018), p. 055107. ISSN: 0034-6748. DOI: 10.1063/1.5019776. URL: https://doi.org/10.1063/1.5019776 (visited on 06/03/2024).

[2] Charles W. Forsberg. "Market Basis for Salt-Cooled Reactors: Dispatchable Heat, Hydrogen, and Electricity with Assured Peak Power Capacity". In: *Nuclear Technology* 206.11 (Nov. 2020). Publisher: Taylor & Francis _eprint: https://doi.org/10.1080/00295450.2020.1743628, pp. 1659–1685. ISSN: 0029-5450. DOI: 10.1080/00295450.2020.1743628. URL: https://doi.org/10.1080/00295450.2020.1743628 (visited on 04/03/2024).

[3] Vladimir D. Golyshev. "High-temperature thermophysical properties of nonscattering semitransparent materials I: methods and instrumentation for the determination of spectral absorptivity and thermal conductivity of melts". In: 4 (1992), pp. 367–377. ISSN: 0018-1544.

[4] K. J. Hollenbeck. *INVLAP.M: A MATLAB Function for Numerical Inversion of Laplace Transforms by the de Hoog Algorithm*. MATLAB code available at: http://www.isva.dtu.dk/staff/karl/invlap.htm. 1998. URL: http://www.isva.dtu.dk/staff/karl/invlap.htm.

[5] F. R. de Hoog, J. H. Knight, and A. N. Stokes. "An Improved Method for Numerical Inversion of Laplace Transforms". In: *SIAM Journal on Scientific and Statistical Computing* 3.3 (1982), pp. 357–366. DOI: 10.1137/0903022.

[6] Na Li et al. "Evaluation of Thermal-Physical Properties of Novel Multicomponent Molten Nitrate Salts for Heat Transfer and Storage". en. In: *Energies* 15.18 (Jan. 2022). Number: 18 Publisher: Multidisciplinary Digital Publishing Institute, p. 6591. ISSN: 1996-1073. DOI: 10.3390/en15186591. URL: https://www.mdpi.com/1996-1073/15/18/6591 (visited on 05/12/2023).

[7] Jared Magnusson, Matthew Memmott, and Troy Munro. "Review of thermophysical property methods applied to fueled and un-fueled molten salts". In: *Annals of Nuclear Energy* 146 (Oct. 2020), p. 107608. ISSN: 0306-4549. DOI: 10.1016/j.anucene.2020.107608. URL: https://www.sciencedirect.com/science/article/pii/S0306454920303066 (visited on 11/23/2023).

[8] Denis Maillet. *Thermal quadrupoles : solving the heat equation through integral transforms*. Wiley, 2000. URL: https://cir.nii.ac.jp/crid/1130282269005111552.

[9] B. Merritt et al. "Measurements of the thermal conductivity of reference liquids using a modified transient hot-wire needle probe". In: *International Journal of Heat and Mass Transfer* 189 (June 2022), p. 122674. ISSN: 0017-9310. DOI: 10.1016/j.ijheatmasstransfer.2022.122674. URL: https://www.sciencedirect.com/

science/article/pii/S0017931022001569 (visited on 10/18/2023).

[10] Brian Merritt. "Modified Transient Hot-Wire Needle Probe for Experimentally Measuring Thermal Conductivity of Molten Salts". In: *Theses and Dissertations* (Oct. 2022). URL: https://scholarsarchive.byu.edu/etd/9733.

[11] Brian Merritt et al. "Thermal Conductivity Characterization of Fluoride and Chloride Molten Salts Using a Modified Transient Hot-Wire Needle Probe". en. In: *International Journal of Thermophysics* 43.10 (Aug. 2022), p. 149. ISSN: 1572-9567. DOI: 10.1007/s10765-022-03073-2. URL: https://doi.org/10.1007/s10765-022-03073-2 (visited on 05/12/2023).

[12] Hiroyasu Mochizuki. "Neutronics and thermal-hydraulics coupling analyses on transient and accident behaviors of molten chloride salt fast reactor". In: *Journal of Nuclear Science and Technology* 60.6 (June 2023). Publisher: Taylor & Francis _eprint: https://doi.org/10.1080/00223131.2022.2131647, pp. 642–668. ISSN: 0022-3131. DOI: 10.1080/00223131.2022.2131647. URL: https://doi.org/10.1080/00223131.2022.2131647 (visited on 04/03/2024).

[13] Valentim M.B. Nunes et al. "Importance of accurate data on viscosity and thermal conductivity in molten salts applications". In: *Journal of Chemical and Engineering Data* 48.3 (2003). Publisher: American Chemical Society, pp. 446–450. ISSN: 00219568. DOI: 10.1021/je0201601.

[14] PDE Solutions Inc. *FlexPDE 7*. Finite element modeling software. n.d. URL: https://www.pdesolutions.com/.

[15] Nick Termini et al. *An Overview of the Molten Salt Thermal Properties Database–Thermophysical, Version 2.1.1 (MSTDB-TP v.2.1.1)*. English. Tech. rep. ORNL/TM-2023/2955. Oak Ridge National Laboratory (ORNL), Oak Ridge, TN (United States), July 2023. DOI: 10.2172/1988348. URL: https://www.osti.gov/biblio/1988348 (visited on 10/26/2023).

[16] Zhitong Yao, Jinhui Li, and Xiangyang Zhao. "Molten salt oxidation: A versatile and promising technology for the destruction of organic-containing wastes". In: *Chemosphere* 84.9 (Aug. 2011), pp. 1167–1174. ISSN: 0045-6535. DOI: 10.1016/j.chemosphere.2011.05.061. URL: https://www.sciencedirect.com/science/article/pii/S0045653511006321 (visited on 04/03/2024).

[17] Qiye Zheng et al. "Advances in thermal conductivity for energy applications: a review". en. In: *Progress in Energy* 3.1 (Feb. 2021). Publisher: IOP Publishing, p. 012002. ISSN: 2516-1083. DOI: 10.1088/2516-1083/abd082. URL: https://dx.doi.org/10.1088/2516-1083/abd082 (visited on 02/22/2024).

A Derivation of Radial to Radial-Axial Ratio Flux Vector

$$\dot{W}_{total} = \sqrt{\dot{W}_{radial}^2 + \dot{W}_{axial}^2} \tag{4}$$

$$\frac{\dot{W}_{total}}{\dot{W}_{axial}} = \sqrt{(\frac{\dot{W}_{radial}}{\dot{W}_{axial}})^2 + 1} \tag{5}$$

$$\dot{W}_{axial} = \frac{\dot{W}_{total}}{\sqrt{(\dot{W}_{radial}/\dot{W}_{axial})^2 + 1}} \tag{6}$$

$$\dot{W}_{radial} = \frac{\dot{W}_{radial}}{\dot{W}_{axial}} * \dot{W}_{axial} \tag{7}$$

$$\dot{W}_{radial} = \frac{\dot{W}_{radial}}{\dot{W}_{axial}} * \frac{\dot{W}_{total}}{\sqrt{(\dot{W}_{radial}/\dot{W}_{axial})^2 + 1}} \tag{8}$$

$$\dot{W}_{radial} = \dot{W}_{total} * \frac{\dot{W}_{radial}/\dot{W}_{axial}}{\sqrt{\dot{W}_{radial}^2/\dot{W}_{axial}^2 + 1}} \tag{9}$$

B Figures and Plots

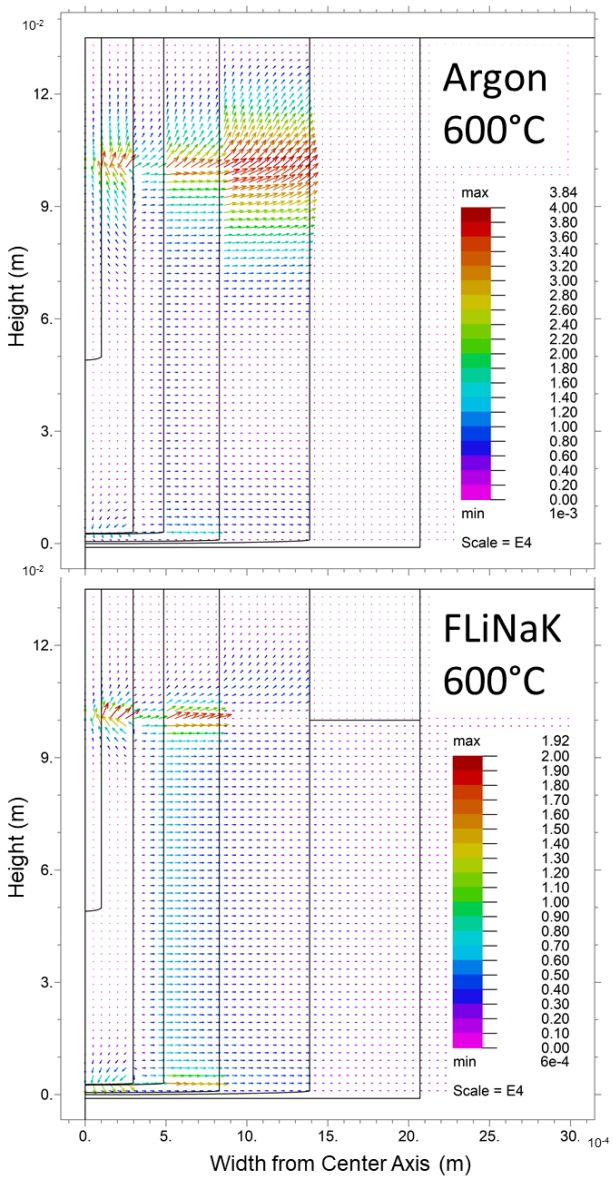

Figure 8: Heat Flux Distribution of argon and FLiNaK at 600 °C.

C FlexPDE Code for FLiNaK

```
TITLE 'Needle Probe Radial X-Section (non-lumped properties)'

COORDINATES YCYLINDER("R","Z") {Rotational Axis "y"}

VARIABLES        { system variables }
  temp              { finding temperature in experiment }

DEFINITIONS
{Geometry Parameters}
r_tc = 0.1e-3 !0.094313e-3                                  ! Radius of Thermocouple
TC_loc = 0.05                             ! Location of TC Bead w relation to probe tip (5 cm)
r_wires = 0.094313e-3                     ! Radius of heating wires
r_wir_o = 0.485942e-3                     ! Outside radius of heating wires
r_wir_i = 0.297315e-3                       ! Inside radius of heating wires
HW_curve = 4.85942e-4                     ! Depth of heating wire curve
HW_Ni = 0.002                            ! Distance between heating wire tip and inner Ni sheath
r_Al = 0.8293e-3                            ! Alumina Layer (in meters)
r_Ni = 1.388E-3                             ! Nickel Sheath (in meters)
Ni_curve = 0.001                          ! Depth of Ni Sheath curved tip
samp_probe = -0.001                       ! Distance between Sample and Probe tip (negative due to
    it being BELOW probe tip)
r_samp = 0.00207                          ! Sample Radius (in meters)
r_cruc = 0.0127                           ! Radius of Crucible (in meters)
h_max = 0.1                              ! Height of Testing Region of Probe (m)
h_cruc = 0.135
length = h_cruc - h_max                                  ! Length above heating wire
h_base = -0.01 + samp_probe                               ! Total area below the probe (Bottom
    Crucible + sample/probe separation)

{Materials defined in each region}
k                                         ! Thermal conductivity of argon (W/mK)
rho                                         ! Density of each layer (kg/m^3)
cp                                        ! Specific heat of each layer (J/kgK)

{ Heating Wire q_gen Calculation Calculations }
phi =0/100                                ! Porosity of cracked alumina
V = 4.351542                                                  ! Voltage going through heating
     wires
I = 0.87532                                                     ! Current going through
    heating wires
vol_wires = pi*r_wires^2*(h_max*2)              ! Calculating Volume of heating wires
L = h_max - ( r_Ni - r_Al + HW_Ni + HW_curve) ! Length of wires (Total length - spacing)
k_wire=17.5704                                               ! Thermal Conductivity of heating
    wires
rho_wire=8670                                           ! Density of Heating Wires
cp_wire=427.07                                         ! Specific Heat of heating wires
q_gen_wire = (V*I)/vol_wires                           ! Heat Generation of WIres
ramp_width = 0.0001

{ Alumina Thermo Properties Calculations }
k_Al = 35.8168*exp((-1.5*phi)/(1-phi))            ! Thermal Conductivity of Alumina
rho_Al=3900                                                  ! Density of Alumina (SHOULD ADD
    POROSITY HERE)
cp_Al=804.8495                            ! Specific Heat of Alumina (SHOULD ADD POROSITY)

```



```
{ General Heat transfer properties }
q_gen  = 0                                ! Heat generation rate in the innermost cylinder (W/m^3)
h_conv = 10                               ! Convective heat transfer coefficient (W/m^2K)
T_amb = 273+020                          ! Ambient temperature (K)
sigma = 5.67e-8                           ! Stefan-Boltzmann constant
e_Ni = 0.35                               ! Emmissivity of Nickel
e_SS = 0.38                              ! Emmissivity of Stainless Steel
rTh_sample_crucible = 1e-3                ! Thermal contact resistance between sample and crucible
rTh_sheath_sample = 1e-3                  ! Thermal contact resistance between dample and sheath
rTh_alumina_sheath = 0.001                ! Thermal contact resistance between alumina and sheath
rTh_wires_alumina = 0.0052                ! Thermal contact resistance between alumina and wires

{ Lumped Probe Properties }
k_probe =  32.0966                        ! Calculated outside of flexPDE for simplicity sake (see below equations)
cp_probe =  784.4098
rho_probe =  3.8998e+03
qgen_probe =  1.9648e+08

{ Lumped Heating Wire Properties Calculation }
k_lump = ((2.0595e-10 + L*4.0826e-8)*k_Al + (3.4381e-11 + L*5.5889e-9)*k_wire) / (4.119e-10 + L*8.1652e-8)
rho_lump = ((2.0595e-10 + L*4.0826e-8)*rho_Al + (3.4381e-11 + L*5.5889e-9)*rho_wire) / (4.119e-10 + L*8.1652e-8)
cp_lump = ((2.0595e-10 + L*4.0826e-8)*cp_Al + (3.4381e-11 + L*5.5889e-9)*cp_wire) / (4.119e-10 + L*8.1652e-8)
qgen_lump = ((3.4381e-11 + L*5.5889e-9)*q_gen_wire) / (4.119e-10 + L*8.1652e-8)

{Radiation}
temp_r2 = EVAL(temp,r_Ni,TC_loc)
temp_r3 = EVAL(temp,r_samp,TC_loc)
q_rad = (sigma*(temp_r2^4 - temp_r3^4)/(1/e_Ni + (1-e_SS)/e_SS * r_Ni/r_samp))

{Time-related parameters}
time_end = 100                            ! Simulation end time (seconds)
t_step = .1                              ! Time step (seconds)

{Heat flux calculations} ! Multiply by 2 since we're only looking at half a probe
top_flux = 2*SURF_INTEGRAL((-k*dz(temp)), 'Top Surface')
bottom_flux = 2*SURF_INTEGRAL((k*dz(temp)), 'Bottom Surface')
cylindrical_flux = 2*SURF_INTEGRAL((-k*dr(temp)), 'Cylindrical Surface')

top_flux_all = 2*SURF_INTEGRAL((-k*dz(temp)), 'Top Surface All')
bottom_flux_all = 2*SURF_INTEGRAL((k*dz(temp)), 'Bottom Surface All')
cylindrical_flux_all = 2*SURF_INTEGRAL((-k*dr(temp)), 'Cylindrical Surface All')

AreaTopBottom = 2*SURF_INTEGRAL(1, 'Top Surface')
AreaTopBottomAll = 2*SURF_INTEGRAL(1, 'Top Surface All')
AreaCylinder = 2*SURF_INTEGRAL(1, 'Cylindrical Surface')
AreaCylinderAll = 2*SURF_INTEGRAL(1, 'Cylindrical Surface All')
AreaTotal = 2*SURF_INTEGRAL(1, 6)


total_flux = 2*SURF_INTEGRAL(normal(-k*grad(temp)),6)

```



```
101
102 {System modifiers}
103 !mesh_spacing = 0.5
104
105 { Give Spec. Materials Spec. Variables }
106 MATERIALS!          Thermal Cond.    Density             Specific Heat            Q-Generation if
        applicable
107   "Crucible" :        k=13.3007   rho=7977      cp=474.5
108     "Sample" :        k=0.78    rho=2034.5      cp=1904.2     ! FLiNaK 600C
109     "Atmosphere":     k=0.0398  rho=0.5525        cp=536      ! argon  600 C
110     "Sheath" :        k=69.5763   rho=8882.8      cp=449.7494
111     "Alumina" :         k=k_Al    rho=rho_Al      cp=cp_Al
112   "Heating_wires" : k=k_lump  rho=rho_lump    cp=cp_lump        !q_gen = qgen_lump
113     "Heating_wires_non" : k=k_lump  rho=rho_lump    cp=cp_lump
114     "Thermocouple" :  k=22.576  rho=8640      cp=450
115     "Probe":          k=k_probe   rho=rho_probe   cp=cp_probe     q_gen=qgen_probe
116
117
118 { Set initial temp: T_amb in definitions }
119 INITIAL VALUES
120   temp = T_amb
121
122 { Heat Eqt with a Source (q_gen) }
123 EQUATIONS
124   temp: div(k*grad(temp)) + q_gen = (rho*cp)*dt(temp)
125
126
127 {Defining the geometry}
128 BOUNDARIES
129
130   { Crucible Region }
131   REGION 1
132   USE MATERIAL "Crucible"             { Makes a big rectanlge to fill entire system }
133     !mesh_spacing = 50                  ! Adjust mesh THIS DOES NOT WORK, TRY TO CHANGE FOR
          EFFICIENCY
134     START (0, h_base)                                  { Bottom Left }
135       value(temp) = T_amb                  ! Set bottom of Crucible to constant temp
136         LINE to (r_cruc, h_base)           { Extends crucible from bottom left to bottom right }
137         natural(temp) = h_conv*(T_amb - temp)  ! Set outer crucible boundary flux to dif./conv.
              equation
138         LINE to (r_cruc, h_cruc)             { Bottom right to top right }
139         natural(temp) = h_conv*(T_amb - temp)  ! Set top crucible boundary flux to dif./conv.
              equation
140         LINE to (0, h_cruc)                    { Top right to top left }
141         natural(temp) = 0                    ! Set inner surface to 0 Flux
142         LINE to CLOSE                        { Close Geometry with a line from top left to bottom
              left }
143
144   { Atmosphere Above Sample Region }
145   REGION 2
146   USE MATERIAL "Atmosphere"             { Makes a rectangular atmosphere which is inserted into
          crucible region }
147     START(0, samp_probe)              { Sets bottom left of rectangle at variabled distance below
           probe tip }
148         LINE to (r_samp, samp_probe)      { Bottom Left to Bottom Right }
149         LINE to (r_samp, h_cruc)          { Bottom Right to Top Right }
150         natural(temp) = h_conv*(T_amb - temp)  ! Set Top  convection boundary
```



```
      LINE to (0, h_cruc)              { Top Right to Top Left }
      natural(temp) = 0                ! Inner Flux to Zero
      LINE to CLOSE                  { Close Geo with a line from Top Left to Bottom Left }

{ Sample Region }
REGION 3
USE MATERIAL "Sample"             { Makes a rectangular sample which is inserted into crucible region }
  START(0, samp_probe)              { Sets bottom left of rectangle at variabled distance below probe tip }
      LINE to (r_samp, samp_probe)     { Bottom Left to Bottom Right }
      LINE to (r_samp, h_max)          { Bottom Right to Top Right }
      LINE to (0, h_max)               { Top Right to Top Left }
      natural(temp) = 0                ! Set Inner Flux to Zero
      LINE to CLOSE                  { Close Geo with a line from Top Left to Bottom Left }


{ Sheath Shell Region }
REGION 4
USE MATERIAL "Sheath"                { Forms 2D slice of sheath: bottom left going CCW }
  START(0, 0)                           { Origin center as bottom left of probe}
      natural(temp) = q_rad               ! Set Probe/Sample interfacing surfaces to have radiating flux
      !Contact(temp) = (1/rTh_sheath_sample) * JUMP(temp)
      ARC (center = 0,Ni_curve) to (r_Ni, Ni_curve) { Bottom Arc to reach outer straight of Probe }
      LINE to (r_Ni, h_cruc)                { Sets Right Straight-Up Portion of Probe }
      natural(temp) = 0                   ! Set Top flux to zero
      LINE to (r_Al, h_cruc)                { Top Right to Top left of top surface }
      NOBC(temp)                        ! Leave undefined flux on inner surface of probe
      LINE to (r_Al, Ni_curve)                  { Inner straight-down bound of Sheath }
      ARC (center = 0,Ni_curve) to (0, r_Ni - r_Al)   { Inner sheath arc (thickness of sheath = (r_Ni - r_Al) }
      natural(temp) = 0                           ! Inner 0 bound flux to zero
    LINE to CLOSE                    { Close Geometry by connecting the arcs on the left zero border }

{ Alumina Region }
REGION 5
USE MATERIAL "Alumina"                 { Creates Alumina inside to Ni sheath }
  START(0, r_Ni - r_Al)                                      { Start Bottom left right above the inner sheath }
      Contact(temp) = (1/rTh_alumina_sheath) * JUMP(temp) ! Add thermal contact res. between Al and Ni
    ARC (center = 0,Ni_curve) to (r_Al, Ni_curve) { Curves around bottom curve of inner sheath }
      LINE to (r_Al, h_cruc)                        { Fixes far right bound of Al }
      natural(temp) = 0                     ! Set top and left bounds to zero flux
      LINE to (0, h_cruc)                     { Top bound }
      LINE to CLOSE                        { Close Geometry with a line from top left to bottom left }

{ Heating Wire Heating Region }
REGION 6
USE MATERIAL "Heating_wires"                     { Forms 2D slice of HWs: Bottom left going CW }
```



```
    q_gen = qgen_lump*URAMP( -z+h_max, -z+(h_max-ramp_width) )    { Cuts off heat generation at
        10cm height }
    !q_gen = swage((z-h_max),qgen_lump ,0,ramp_width)
    START(0, r_Ni - r_Al + HW_Ni )                          { Bottom Left (Sheath thickness + HW/Ni
         Dist.) }
        natural(temp) = 0                                  ! Set the left zero bound to zero flux
      LINE to (0, r_Ni - r_Al + HW_Ni + r_wires*2)           { Inner left zero bound of wire }
        NOBC(temp)                                      ! Reset BC for inner HW
      !Contact(temp) = (1/rTh_wires_alumina) * JUMP(temp) ! Add Contact Res. between HW and Al
                                                       { Inner arc of Heating wire }
        ARC (center = 0, r_Ni - r_Al + HW_Ni + HW_curve) to (r_wir_i, r_Ni - r_Al + HW_Ni +
            HW_curve)
        LINE to (r_wir_i, h_cruc)                          { Inner staight up bound of HW }
        natural(temp) = 0                                  ! Set top bounds to 0 flux
        LINE to (r_wir_o, h_cruc)                          { Line Top Left to Top Right on HW top
            bounds }
        NOBC(temp)                                      ! Reset BC for inner HW
        !Contact(temp) = (1/rTh_wires_alumina) * JUMP(temp) ! Add Contact Res. between HW and Al
    LINE to (r_wir_o, r_Ni - r_Al + HW_Ni + HW_curve)   { Outer straight-down bound of HW }
        ARC (center = 0,  r_Ni - r_Al + HW_Ni + HW_curve) to CLOSE { Close Geo by using final arc
             to bot. Left }

  { Thermocouple Region }
  REGION 7
  USE MATERIAL "Thermocouple"                     { Forms TC by rect. with arc bottom to create
      bead }
    START(0, h_cruc)                                 { Start at the top left bound }
      natural(temp) = 0                                ! Set top BC of TC to zero
      LINE to (r_tc, h_cruc)                           { Top Left to Top Right }
        NOBC(temp)                                   ! Reset BC for outer TC
      !Contact(temp) = (1/rTh_wires_alumina) * JUMP(temp) ! Cont Res. between TC and Al. FIX TO
          BE WITH CHROMEL
        LINE to (r_tc, TC_loc)                           { Outer straight-down bound of TC }
        ARC (center = 0, TC_loc)  to (0, TC_loc - 0.001)          { Arc to inner zero bound (TC
            Bead formation) }
        natural(temp) = 0                                  ! Set inner zero-bound of TC to zero flux
        LINE to CLOSE                                 { Close Geo by far left inner closing bot.
            left to top left }

! Box enclosing heater portion
  FEATURE "Top Surface"
    START(0, h_max+ramp_width) LINE to (r_wir_o, h_max+ramp_width)

  FEATURE "Bottom Surface"
    START(0, r_Ni - r_Al + HW_Ni )  LINE to (r_wir_o, r_Ni - r_Al + HW_Ni )

 FEATURE "Cylindrical Surface"
    START(r_wir_o, h_max+ramp_width)  LINE to (r_wir_o,  r_Ni - r_Al + HW_Ni )


!Surfaces enclosing heater portion, extending to end of everything

 FEATURE "Top Surface All"
    START(r_cruc, h_max+ramp_width) LINE to (0, h_max+ramp_width)

  FEATURE "Bottom Surface All"
    START(0, r_Ni - r_Al + HW_Ni )  LINE to (r_cruc, r_Ni - r_Al + HW_Ni )
```



```
 FEATURE "Cylindrical Surface All"
    START(r_wir_o, h_cruc)  LINE to (r_wir_o, 0.001 )


{ Set the time bounds for plots monitors histories, etc. values are variables but this helps
    FlexPDE know }
TIME
0 BY t_step TO time_end


!MONITORS

! No needed Monitors at this time

PLOTS
  FOR t = 0 BY t_step TO time_end

    { Creating the Heat Flux Field: See zoom names for details on zoom }
    !vector(-K*dr(Temp), -K*dz(temp)) as "Overall Heat Flux Field"
  !vector(-K*dr(Temp), -K*dz(temp))  zoom(0.0,-0.001, 0.021,0.02) as "Heat Flux Probe Tip"
  !vector(-K*dr(Temp), -K*dz(temp))  zoom(0.0,0.045, 0.0023,0.06) as "Heat Flux Sensing Region"
    vector(-K*dr(Temp), -K*dz(temp))  zoom(0.0, 0.0, .003, h_cruc) as "Heat Flux Total Probe"
        export format "#t#r,#i" file="TopFlux.txt"

    { Countour maps of heat: See zoom names for details on zoom }
    !CONTOUR(temp) as "Contour Temp"
    !contour(Temp) zoom(0.0,-0.001, 0.021,0.02) as "Countour Temp Probe Tip"
  !contour(Temp) zoom(0.0,0.045, 0.0023,0.06) as "Countour Temp Sensing Region"
    contour(Temp) zoom(0.0, 0.0, .003, h_cruc) as "Countour Temp Total Probe"

    { Shows temperature profile at 0.05 cm (at TC Bead) from 0 (TC) into crucible (but not all
        the way) }
    elevation(Temp) from (0,0.05) to (0.0025,0.05) as "Temp Profile"

    elevation(-k*dr(Temp)) on "Cylindrical Surface" as "Flux Rad Profile"
    elevation(-k*dz(Temp)) on "Top Surface" as "Flux Top Ax Profile"
    elevation(-k*dz(Temp)) on "Bottom Surface" as "Flux Bottom Ax Profile"

    elevation(-k*dr(Temp)) on "Cylindrical Surface All" as "Flux Rad Profile All"
    elevation(-k*dz(Temp)) on "Top Surface All" as "Flux Top Ax Profile All"
    elevation(-k*dz(Temp)) on "Bottom Surface All" as "Flux Bottom Ax Profile All"


   {elevation(top_flux) as "Top Flux Over Time"
   elevation(bottom_flux) as "Bottom Flux Over Time"
   elevation(cylindrical_flux) as "Cylindrical Flux Over Time"
}

!REPORT(SURF_INTEGRAL(normal(-k*grad(temp)), "Cylindrical Surface")) AS "Cylindrical Heat Flux"



HISTORIES

   history(top_flux) as "Top Heat Flux (W)" export format "#t#r,#i" file="TopFlux.txt"
   history(bottom_flux) as "Bottom Heat Flux (W)" export format "#t#r,#i" file="BottomFlux.txt"
```



```
    history(cylindrical_flux) as "Cylindrical power output (W)" export format "#t#r,#i" file="
        FLiNaK_CylindricalFlux.txt"
    history((cylindrical_flux_all/AreaCylinderAll)/((top_flux_all+bottom_flux_all)/
        AreaTopBottomAll)) as "Ratio Radial to Axial Flux (W/mK)" export format "#t#r,#i" file="
        FLiNaK_Radial_to_Axial_Flux.txt"

    history(-k*dr(Temp)) at (r_Ni, TC_loc) as "Heat Flux at TC-Outer Probe, radial (W/mK)" export
        format "#t#r,#i" file="TC-ProbeFluxRad.txt"
    history(-k*dz(Temp)) at (r_tc, TC_loc+0.00) as "Heat Flux at 0-TC, axial (W/mK)" export format
         "#t#r,#i" file="0-TCFluxAx.txt"
    history((top_flux_all+bottom_flux_all)/AreaTopBottomAll) as "Avg Heat Flux, axial (W/mK)"
        export format "#t#r,#i" file="AvgFluxAx.txt"

    !history(bottom_flux/AreaTopBottom) as "Bottom Avg Heat Flux (W)" export format "#t#r,#i" file
        ="TC-ProbeAvgFluxAx.txt"
    !history(-k*dz(Temp)) at (r_Ni, TC_loc) as "Heat Flux at TC-Outer Probe, axial (W/mK)" export
        format "#t#r,#i" file="TC-ProbeluxAx.txt"

    history(-k*dr(Temp)) at (r_wir_o, TC_loc) as "Heat Flux at TC-Outer HW, radial (W/mK)" export
        format "#t#r,#i" file="TC-HWFluxRad.txt"
    history(cylindrical_flux/AreaCylinder) as "Avg Heat Flux, radial (W/mK)" export format "#t#r,#
        i" file="AvgFluxRad.txt"
    history(cylindrical_flux_all/AreaCylinderAll) as "Avg Heat Flux All, radial (W/mK)" export
        format "#t#r,#i" file="AvgFluxRadAll.txt"









    !history(bottom_flux_all/AreaTopBottomAll) as "Bottom Avg Heat Flux (W)" export format "#t#r,#
        i" file="TC-ProbeAvgFluxAx.txt"
    !history(-k*dz(Temp)) at (r_wir_o, TC_loc) as "Heat Flux at TC-Outer HW, axial (W/mK)" export
        format "#t#r,#i" file="TC-HWFluxAx.txt"

    history(total_flux) as "Total Flux" export format "#t#r,#i" file="TotalFlux.txt"

  { History of Temps at the following points:
    a. TC
    b. Middle of HW
    c. Middle(ish) of Sample }
    History(Temp) AT (0.0, 0.05) export format "#t#r,#i" file="temp.txt"

END
```

Listing 1: Needle Probe Radial X-Section (non-lumped properties)

